PCCP

PAPER

View Article Online
View Journal | View Issue

Cite this: *Phys. Chem. Chem. Phys.*, 2018, **20**, 29513

Computational characterization of the selective inhibition of human norepinephrine and serotonin transporters by an escitalopram scaffold†

Guoxun Zheng,[ab] Fengyuan Yang,[ab] Tingting Fu,[ab] Gao Tu,[ab] Yuzong Chen,[c] Xiaojun Yao,[d] Weiwei Xue*[b] and Feng Zhu*[ab]

Received 7th October 2018,
Accepted 30th October 2018

DOI: 10.1039/c8cp06232c

rsc.li/pccp

Human norepinephrine and serotonin transporters (hNET and hSERT) are closely related monoamine transporters (MATs) that regulate neurotransmitter signaling in neurons and are primary targets for a wide range of therapeutic drugs used in the treatment of mood disorders. The subtle modifications of an escitalopram scaffold exhibit distinct selective inhibition profiles of hNET and hSERT. However, the structural details of escitalopram scaffold binding to hSERT and (or) hNET are poorly understood and still remain a great challenge. In this work, on the basis of more recently solved X-ray crystallographic structure of hSERT in complex with escitalopram, 3 μs long all-atom MD simulations and binding free energy calculations *via* MM/GB(PB)SA, thermodynamic integration (TI) and MM/3D-RISM methods were performed to reproduce experimental free energies. And both MM/GBSA and TI have a high correlation coefficient (R^2 = 0.95 and 0.96, respectively) between the relative binding free energies of the calculated and experimental values. Furthermore, MM/GBSA per-residue energy decomposition, molecular interaction fingerprints and thermodynamics–structure relationship analysis were employed to investigate and characterize the selectivity of the escitalopram scaffold with three modifications (escitalopram, ligand**10** and talopram) to hNET and hSERT. As a result, 4 warm spots (A73, Y151, A477 and I481) in hNET and 4 warm spots (A96, A173, T439 and L443) in hSERT were thus discovered to exert a pronounced effect on the selective inhibition of hNET and hSERT by the studied ligands. These simulation results would provide great insight into the design of inhibitors with the desired selectivity to hNET and hSERT, thus further promoting the research of more efficacious antidepressants.

Introduction

The design of small molecules with the appropriate selective inhibitory mechanism to desired targets is a continual challenge in drug discovery, especially for proteins from the same family, such as G protein-coupled receptors (GPCRs), kinases, membrane channels and transporters.[1–3] Human norepinephrine and serotonin transporters (hNET and hSERT) are closely related monoamine transporters (MATs) regulating the reuptake of norepinephrine (NE) or 5-hydroxytryptamine (5-HT) from the extracellular space into the neuron.[4–7] They are primary therapeutic targets for a wide range of drugs used for treating mental disorders caused by the imbalances in neurotransmitter homeostasis.[8–10] Tricyclic antidepressants (TCAs) are the first discovered medications targeting hNET and hSERT, but their broad activities across various other neurotransmitter receptor systems often lead to severe side effects.[11–13] Recently, second-generation antidepressants, such as selective serotonin reuptake inhibitors (SSRIs), selective norepinephrine reuptake inhibitors (NRIs) and serotonin and norepinephrine reuptake inhibitors (SNRIs),[14,15] have been widely applied as the first-line therapy for major depression.[16]

Clinical trial treatments suggested that balancing and regulating the inhibitory activities of hSERT and (or) hNET is viable for achieving the optimal therapeutic properties for SSRIs, NRIs and SNRIs,[17] which has been used in an increasing number of personal therapeutic applications.[18] It is interesting that an escitalopram scaffold has been developed as a powerful and privileged probe to explore the inhibitor selectivity to hNET

[a] *College of Pharmaceutical Sciences, Zhejiang University, Hangzhou 310058, China. E-mail: zhufeng@zju.edu.cn, prof.zhufeng@gmail.com; Tel: +86 (0)571 8820-8444*
[b] *School of Pharmaceutical Sciences and Collaborative Innovation Center for Brain Science, Chongqing University, Chongqing 401331, China. E-mail: xueww@cqu.edu.cn; Tel: +86 (0)23 65678468*
[c] *Bioinformatics and Drug Design Group, Department of Pharmacy, National University of Singapore, Singapore 117543, Singapore*
[d] *State Key Laboratory of Applied Organic Chemistry and Department of Chemistry, Lanzhou University, Lanzhou 730000, China*

† Electronic supplementary information (ESI) available. See DOI: 10.1039/c8cp06232c

	SSRI Escitalopram	SNRI Ligand 10	NRI Talopram
K_i^{hSERT}(nM)	21	542	28108
K_i^{hNET} (nM)	47140	233	16

Fig. 1 Chemical structures of escitalopram, ligand**10** and talopram and their binding affinity (K_i) to hNET and hSERT. The escitalopram scaffold shared by the three ligands is illustrated in green.

and hSERT[19,20] (Fig. 1). Escitalopram is one of the most potent and selective SSRIs.[21] Talopram, obtained from subtle modifications of the escitalopram scaffold, turns out to be one of the most potent and selective NRIs.[15] A structure–activity relationship (SAR) study of the escitalopram scaffold identified ligand**10** (numbered in the work of Andersen *et al.*[19]) as a SNRI with nearly equal affinity for both hNET and hSERT *via* a slight modification of the escitalopram scaffold. The uptake-saturation experiments with hNET and hSERT in the absence or presence of inhibitors indicated that escitalopram, ligand**10** and talopram bound in the central substrate-binding site (S1) located between transmembrane helices (TM) 1, 3, 6, 8 and 10.[19]

More recently, the X-ray crystallographic structure of hSERT in complex with escitalopram revealed that escitalopram locked hSERT in an outward-open conformation by lodging in the S1 site.[22] Additionally, computational simulations shed light on the poses of inhibitors binding to hSERT and (or) hNET.[23] Koldsø *et al.*[24] examined the orientations of the two citalopram enantiomers in hSERT *via* induced fit docking from a LeuT-based homology model.[25] Using the crystal structure of the dopamine transporter from *Drosophila melanogaster* (dDAT)[26] as a template, Xue and Zheng *et al.*[27–30] constructed hSERT and hNET models and explored the binding mechanisms of FDA approved SSRIs, NRIs and SNRIs (including escitalopram and talopram) in their corresponding targets by molecular dynamics (MD) simulation. Although considerable efforts have been made, they are inconclusive to reveal the structural determinates and selectivity of ligands binding to hNET and (or) hSERT. Thus, a deeper understanding of the physicochemical basis underlying the binding specificity of ligands to hNET and hSERT was urgently needed and would provide great insights into the design of potent single- or dual-target inhibitors.

One of the most rigorous approaches for addressing this issue was the long-timescale MD simulation based on protein–ligand binding free energy calculation.[31–36] Using MD trajectories, several approaches can be utilized to calculate the binding free energy including free energy perturbation (FEP),[32–34] thermodynamic integration (TI),[37,38] the molecular mechanics (MM)/3D reference interaction site model (MM/3D-RISM)[39] and the end-state methods such as the molecular mechanics (MM) combined with the Poisson–Boltzmann or generalized Born solvation plus surface area correction (MM/PBSA and MM/GBSA).[40–46] Among them, FET, TI and MM/3D-RISM are more accurate but more computationally demanding. Compared with these methods, the end-state ones deployed for calculating binding free energy are characterized by their relative effectiveness and accuracy.[40,47,48] Herein, we started from the X-ray crystal structure of hSERT in complex with escitalopram[22] and employed all-atom, long-timescale MD simulations followed by the binding free energy calculation (including MM/GB(PB)SA, thermodynamic integration and MM/3D-RISM methods), the MM/GBSA per-residue energy decomposition, molecular interaction fingerprint and thermodynamics–structure relationship analysis to investigate and characterize selective inhibition profiles of 3 ligands binding to their targets. The results shed light on the delicate modifications of a scaffold conferring its distinct affinity and the residues in S1 affecting the selectivity of drugs for the two closely related transporters at atomic levels.

Materials and methods

Construction of the studied complexes

To explore the molecular determinates of selective inhibition of hNET and hSERT by antidepressants, six complexes were constructed (Table 1), which included hNET and hSERT in complex with inhibitors escitalopram, ligand**10** and talopram (Fig. 1). The way to construct complexes is described below:

Table 1 The summary of the simulation systems

Systems	Starting structures	Total atoms	Simulation time (ns)
Talopram-hNET	Talopram docked into hNET	96 198	500
Escitalopram-hSERT	X-ray structure (PDB ID: 5I71)	94 874	500
Ligand**10**-hNET	Ligand**10** docked into hNET	96 192	500
Ligand**10**-hSERT	Ligand**10** docked into hSERT	95 272	500
Talopram-hSERT	Talopram docked into hSERT	94 876	500
Escitalopram-hNET	X-ray structure (5I71) aligned into hNET	94 619	500

Preparation of protein structures. The crystallographic structure of hSERT in complex with escitalopram was obtained from the Protein Data Bank (PDB code: 5I71;[22] resolution: 3.15 Å). There were three mutations (T110A, I91A and T439S) in 5I71, and the mutagenesis tool in PyMOL[49] was used to mutate the structure back to its native state and then preprocessed by Protein Preparation Wizard.[50] The 3D structure of hNET was built by the homology modeling approach in Prime[51] using the modified native hSERT structure as a template. The sequence of hNET was downloaded from UniProt (accession number: P23975[52]). Sequence alignments between hNET and hSERT were performed by ClustalX[53] and visualized by ESPript[54] (Fig. S1, ESI†). To evaluate the stereochemical qualities of the modeled hNET, all-atom contact analysis and high-accuracy Ramachandran plot analysis were conducted, and rotamer distributions were calculated using the MolProbity program.[55]

Docking and optimization of the initial binding pose. The initial structural complex of escitalopram bound to hNET was obtained by directly introducing escitalopram from the modified hSERT-escitalopram complex into the generated hNET homology model. The complex was then subjected to loop refinement and energy minimizations (1000 steps steepest descent with backbone constrained). The complexes of ligand**10** and talopram bound to hNET and hSERT were obtained using molecular docking. Based on the structures of hNET and hSERT in complex with escitalopram, the grid box was first generated using the Receptor Grid Generation in Glide[56] by centering escitalopram in hNET and hSERT. Then, ligand**10** and talopram were docked into the defined grid boxes using the standard precision (SP) scoring algorithm within Glide[56] allowing flexible ligand sampling. The ligands were subjected to LigPrep using the OPLS-2005 force field[57] to generate the low energy conformations, and the ionized state was realized by Epik[58] at a pH value of 7.0 ± 2.0 before docking. The conformation of escitalopram in hNET or hSERT was used as a reference for selecting a reasonable binding pose for ligand**10** and talopram, which were involved in the essential interaction with the corresponding residues shown by previous mutagenesis studies.[59–62] Finally, the binding poses of six complexes were optimized using Prime[58] by considering both the flexibility of ligands and residues around 6.0 Å of the ligands.

Molecular dynamics simulation

System setup. Six complexes were embedded into the explicit hydrated POPC membrane bilayer, forming a periodic cell of each system (96 Å × 96 Å × 117 Å box) containing ~95 000 atoms. The spatial arrangement of the transmembrane transporter with respect to the lipid bilayer was predicted using the PPM web-server.[63] The membrane bilayer was generated using the CHARMM-GUI Membrane Builder,[64] maintaining a water (TIP3P[65]) thickness of 20.0 Å on the top and bottom of the protein, including ion concentrations of 0.15 M Na^+ and Cl^-. The tLEaP tool in AMBER16[66] was applied to construct the force field files and generate the topology and coordinate files for each system. In particular, the protein and lipid were described by ff14SB and Lipid14,[67] respectively. Ion (Na^+ and Cl^-) parameters for TIP3P water were characterized as Joung/Cheatham ion parameters.[68,69] The ligand parameters were assigned as general AMBER force field 2 (gaff2) atom types and the partial charges were derived from RESP calculation using antechamber.[70] Geometry optimization and electrostatic potential calculations for the ligands were performed at the HF/6-31G* level by Gaussian 09.[71]

Energy minimization, equilibration and production run. All simulations were carried out using the AMBER16 suite[66] with GPU-accelerated PMEMD. First, the energetically unfavorable contacts were removed *via* two steps. The first energy minimization step was to apply a harmonic restraint on the lipid and the solute atom (force constant = 10.0 kcal mol^{-1} $Å^{-2}$) and then to release all atoms to move freely in the second step. In each step, the full systems were minimized for 10 000 steps, of which the first 5000 and the remaining steps adopted steepest descent and the conjugate gradient method, respectively. Second, each system was heated from 0 to 100 K and then gradually to 310 K with the protein and lipid restrained over 100 ps in the *NVT* ensembles. Third, 5 ns unrestrained equilibrations (10 times) were performed to equilibrate the system's periodic boundary condition dimension. Finally, the unrestrained 500 ns production simulation was carried out for six systems in the *NPT* ensembles (310 K and 1 atm). The temperature and pressure were controlled using a Langevin thermostat[72] and a Monte Carlo barostat,[66] respectively. The particle-mesh Ewald (PME) method[73] was used to handle the long range electrostatic interactions. The SHAKE algorithm[74] was exploited to keep all bonds (involving hydrogen atoms) rigid. The time step of the simulation was set as 2.0 fs and a 10.0 Å cutoff was used for non-bonded interactions.

Analysis of the simulation trajectory. Based on the MD simulation trajectories of the six systems, the related properties such as root mean square deviation (RMSD) and the representative structures along the MD simulations and binding free energy were analyzed and predicted *via* cpptraj and mm_pbsa.pl programs implemented in AMBER16.[66] Structure visualization was conducted in the PyMOL software.[49]

Binding free energy and per-residue contribution decomposition analysis

MM/GB(PB)SA method. The binding free energies of ligands to hNET or hSERT (ΔG_{calc}) were obtained *via* the MM/GB(PB)SA approach based on the single trajectory. 1000 snapshots extracted from the last 100 ns trajectory of simulations were used for energy calculations. For each snapshot, the energy of ligands binding to hNET or hSERT was computed by eqn (1):

$$\Delta G_{calc} = \Delta E_{vdW} + \Delta E_{ele} + \Delta G_{pol} + \Delta G_{apol} - T\Delta S \quad (1)$$

In eqn (1), ΔE_{vdW}, ΔE_{ele}, ΔG_{pol} and ΔG_{apol} indicate the van der Waals interaction energy, electrostatic energy, polar solvent interaction energy (GB[75] and PB[76] model, igb = 2) and apolar solvation energy (LCPO model, 0.0072 × ΔSASA),[77,78] respectively. Among them, SASA represents the solvent-accessible surface area evaluated by augmenting the radii of all atoms using the probe radius (1.4 Å). $-T\Delta S$ is the entropic penalty calculated *via* a normal mode analysis[79] based on the 10 frames from the last 100 ns trajectory.

The per-residue energy contribution ($\Delta G_{calc}^{per\text{-}residue}$) for ligands binding to hNET or hSERT was computed in the same fashion as the binding free energy calculation *via* MM/GBSA.

$$\Delta G_{calc}^{per\text{-}residue} = \Delta E_{vdW}^{per\text{-}residue} + \Delta E_{ele}^{per\text{-}residue} + \Delta G_{pol}^{per\text{-}residue} + \Delta G_{apol}^{per\text{-}residue} \quad (2)$$

where $\Delta E_{vdW}^{per\text{-}residue}$, $\Delta E_{ele}^{per\text{-}residue}$ and $\Delta G_{pol}^{per\text{-}residue}$ in eqn (2) are defined with the same meanings as the corresponding terms in eqn (1). The difference is that the apolar solvent energy ($\Delta G_{apol}^{per\text{-}residue}$) is modeled by a recursive approximation of a sphere around an atom starting from an icosahedron (ICOSA).[66]

Thermodynamic integration calculation

The thermodynamic integration (TI) method has been regarded as a robust approach to calculate the energy difference between the subtle modification of ligands on the basis of MD simulation.[37] TI simulation has also been applied to calculate the relative binding free energy ($\Delta\Delta G$) of ligand**10** transformed into escitalopram or talopram in hNET and hSERT. This calculation is shown in Scheme 1. The values of $\Delta\Delta G$ were computed *via* three steps including decharge, vdw-bonded and recharge.[80] ΔG of each step was calculated *via* the following eqn (3):

$$\Delta G = \int_0^1 \left\langle \frac{\partial V(\lambda)}{\partial \lambda} \right\rangle_\lambda d\lambda \quad (3)$$

where λ is the coupling parameter, V is λ coupling potential function, and the integration limits 0 and 1 represent two different states that correspond to WT (ligand**10**) and mutations (escitalopram and talopram). The angle brackets indicate the Boltzmann-weighted average. The integral in eqn (3) is solved numerically *via* several simulations with different λ window values ranging from 0.0 to 1.0 based on eqn (4):

$$\Delta G = \sum_{i=1}^{n} W_i \left\langle \frac{\partial V}{\partial \lambda} \right\rangle_{\lambda_i} \quad (4)$$

where the values of λ and their corresponding weights W_i are assigned by using the Gaussian quadratic formula. The potential functions $V(0)$ for $\lambda = 0$ and $V(1)$ for $\lambda = 1$ correspond to the WT (ligand**10**) and the mutation of the ligand. TI calculation is performed for each λ in 3 steps:[80] (1) decharge, charge removal from ligand**10**; (2) vdw-bonded, change of ligand**10** into the mutated ligands (escitalopram and talopram) without electrostatic interaction; (3) recharge, charge addition to the mutated ligands. During the calculation, the soft-core potential is utilized only in the second step to deal with the disappearance and appearance of atoms related to the mutation. The sample space is characterized by 11 different λ values (0.0–1.0). For each λ value, three separate 2 ns MD simulations have been carried out on the WT and the mutated ligands. All of the thermodynamic integration calculations have been realized in AMBER16.[66]

Molecular interaction fingerprint analysis

Based on 1000 snapshots extracted from the final 100 ns simulation, the molecular interaction fingerprints between the protein and ligand were calculated using IChem[81–83] with the default parameters. For each frame, the calculation zones of the complex were defined as the regions within 6 Å of the ligand mass center. During the calculation, seven important pharmacological properties (including hydrophobic, aromatic, h-bond donor, h-bond acceptor, positively ionizable, negatively ionizable and meta) of the atoms of proteins and ligands were evaluated by parsing atoms and bond connectivity fields.[84] The calculated protein–ligand interaction fingerprints of 1000 snapshots were displayed *via* radar charts.

Results and discussion

Homology model of hNET and the S1 binding site

The recently disclosed crystallographic structure of escitalopram bound to hSERT (PDB code: 5I71[22]) was used as a template for hNET homology modeling. The overall sequence identity between hNET and hSERT equaled 54% (Fig. S1, ESI†). Quality evaluations and detailed all-atom contact analyses for the 3D structures of the hNET model are shown in Fig. S2 (ESI†). As shown, 98.0% residues in the hNET model were either in favored or allowed regions of the Ramachandran plot, suggesting that the overall main and side chain conformations were reasonable. Compared to the previously reported hNET models built on the basis of the dDAT structure (PDB code: 4M48[85]), the model herein was built taking the protein conformation with ligands bound

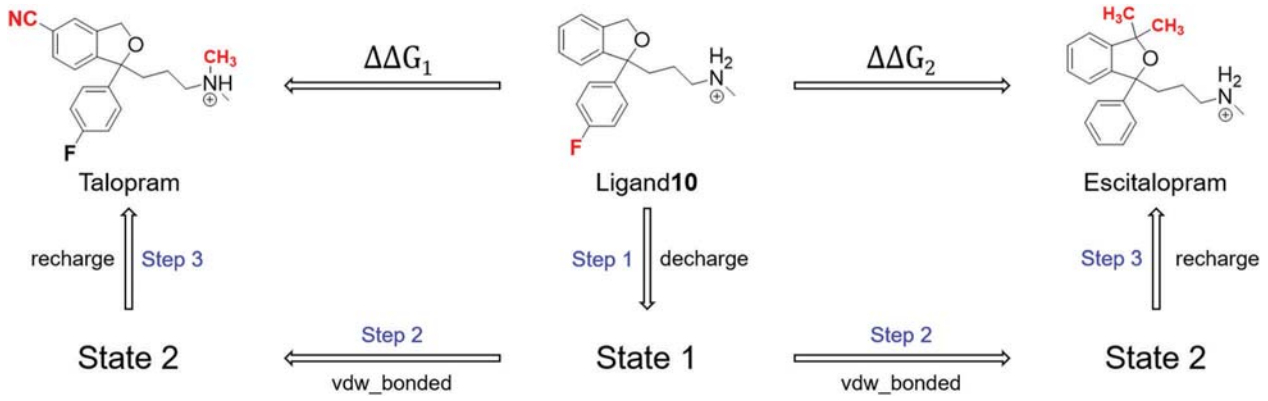

Scheme 1 Thermodynamic process to perform thermodynamic integration.

into consideration. In addition, the S1 binding site identity between hNET and hSERT was 62% (Fig. S1, ESI†) and it was expected that the hSERT-based model could better represent the ligand binding state of hNET. Moreover, the studied ligand**10** and talopram were derived from the subtle modifications of the escitalopram scaffold (Fig. 1). Thus, both the modified hSERT and modeled hNET structures provided an appropriate starting point for investigating the binding of escitalopram, ligand**10** and talopram to their target(s): hNET and hSERT.

Initial poses of escitalopram, ligand10 and talopram complexed with hNET and hSERT

The initial binding pose of escitalopram in the S1 site of hSERT was reported in structure 5I71.[22] To obtain the binding pose of escitalopram in the hNET S1 site, the coordinates of escitalopram in hSERT were directly introduced into the hNET S1 site (Fig. S3, ESI†). As shown, the positively charged nitrogen of the ligands formed salt bridges with the negatively charged residue in those two targets (hNET: D75 and hSERT: D98, both of which played a crucial role in ligand recognizing hNET or hSERT[59]). The initial poses of ligand**10** and talopram binding to hNET and hSERT were predicted by molecular docking. Fig. 2 shows the superimposition of six initial complexes with escitalopram, ligand**10** and talopram as well as the residues around 6.0 Å of the ligands. It was noted that the binding site (S1 site) surrounded by TM1, 3, 6, 8 and 10 was composed of three subsites (A, B and C), and the three subsites accommodated the different parts of the ligands (Fig. 2). The amine group of the ligands occupied subsite A and formed a salt bridge with the carboxylate of the conserved D75 for hNET and D98 for hSERT.[19,22] F72 in hNET and Y95 in hSERT may also form a cation-π interaction with the charged amine group.[59] In addition, S318 in hNET (S336 in hSERT) partnered in an interaction network with the ligands.[86–88] In subsite B, T439 and L443 in hSERT defined a hydrophobic cavity that participated in the hydrophobic interaction with the fluorophenyl or phenyl group of the ligands. Similarly, the fluorophenyl or phenyl group of the ligands was inserted into the hydrophobic cavity (S420 and A145). In subsite C, the cyanophthalane formed an edge-to-face interaction with F317 and F323 (hNET) and F335 and F341 (hSERT). V148, Y151, F317, I481 and F323 in hNET defined mixed surfaces where the cyan group of escitalopram was inserted. Correspondingly, I168, I172, Y175, T497 and V501 in hSERT formed a mixed non-polar/polar surface which accommodated the cyan group of escitalopram.

In addition, the poses of escitalopram, ligand**10** and talopram demonstrated slight shifts in hNET and hSERT (Fig. 2); however, the snapshots of the protein and ligand from the crystallographic and docking methods were stationary and rigid. Fully understanding the key roles of residues in determining selective inhibition of hNET and hSERT by the ligands was still limited. Thus, MD simulation was needed to sample the more reasonable poses from the initial ones, which would reveal the delicately structural and energetic mechanism underlying the selectivity of escitalopram, ligand**10** and talopram binding to their target(s).

Structure dynamics and binding free energy of the complexes

Simulation stability of the complex. To sample the conformation of protein–ligand interactions, 3 μs long (500 ns for each complex) MD trajectories were collected. The root-mean-square deviations (RMSDs) of the whole protein, ligand, binding site (residues around 6.0 Å of ligands), TM domains and loop for the six complexes relative to the corresponding initial coordinates were calculated during the entire simulation (Fig. S4, ESI†). As demonstrated, for all simulated complexes, the average RMSD value of proteins was equal to ~3.0 Å, which was larger

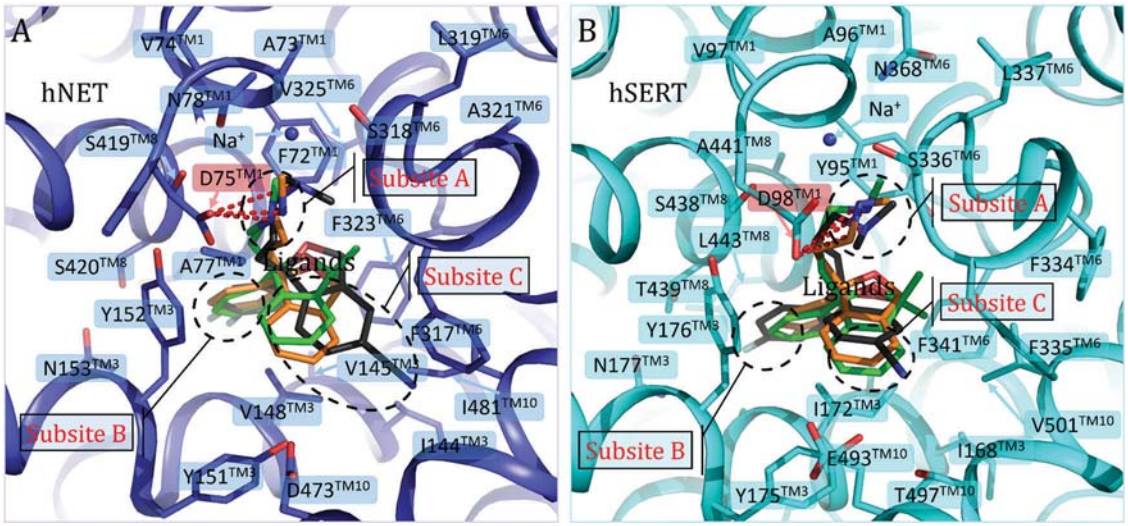

Fig. 2 Structural superimposition of the initial poses of 3 ligands, escitalopram (dark sticks), ligand**10** (orange sticks) and talopram (green sticks) in the S1 site of (A) hNET (in blue cartoon) and (B) hSERT (in cyan cartoon). The side chain of residues in hNET and hSERT around the ligands ~6.0 Å are shown with sticks and the residue names and the corresponding transmembrane (TM) domains are labeled. Three subsites in hNET and hSERT are also marked as Subsite A, Subsite B and Subsite C (in dashed circles), into which the corresponding three moieties of ligands are inserted. The salt bridges between the ligands and residues (D75 in hNET and D98 in hSERT) are displayed in red dashed lines.

than that of the ligands (~1.5 Å) and the binding site (~1.0 Å). The average RMSD value of TM domains was less than 1.5 Å, while the loop regions underwent relatively larger fluctuations (2.8–3.5 Å). It is worth noting that the ligands and the binding site residues in both hNET and hSERT have a similar fluctuation range along the simulation (Fig. S4, ESI†), indicating that the ligands and the binding site residues sampled a more reasonable conformation to accommodate each other. Additionally, compared to TM1, 3, 6, 8 and 10, low fluctuations of the binding sites suggested that the ligands could stabilize the residues.

Representative snapshots of the complexes. The representative snapshots of escitalopram, ligand**10** and talopram binding to hNET and hSERT were extracted from the last 100 ns equilibrium trajectories and were aligned to their corresponding initial poses (Fig. S5, ESI†). The representative snapshots were extracted *via* three steps. First, we calculated the average structures (pseudo structures) of each complex based on the main chain atoms (CA, C and N) during the trajectories of the last 100 ns simulations. Second, the RMSDs of 1000 snapshots extracted every 10 intervals aligned to the pseudo average structures were calculated and then ordered based on the RMSD values. Third, the snapshots with the minimal RMSDs to the average structure were extracted as the representative snapshots. As shown, there were three key interactions within all of the six complexes. From the initial structures, one of the three key interactions (salt bridge) was maintained very well. Escitalopram, ligand**10** and talopram were all anchored by the conserved salt bridge between the charged amine group and the carboxyl of D75 in hNET (Fig. S5A–C, ESI†) and D98 in hSERT (Fig. S5A′–C′, ESI†) in subsite A. As for the other two key interactions, the fluorophenyl or phenyl group of the ligands was inserted into subsite B, and the cyanophthalane or phthalane orientated to subsite C. The side chain of the residues and moieties of the ligands related to the two hydrophobic interactions underwent some conformational changes (Fig. S5, ESI†), and the calculated RMSD value was ~2.0 Å.

Binding free energy of the complex. Herein, three methods including approximate MM/GB(PB)SA and more rigorous TI and MM/3D-RISM were utilized to calculate the free energy and reproduce the experimental free energy of the studied protein–ligand complex. Firstly, the free energies (ΔG_{calc}) of ligands binding to hNET and hSERT calculated *via* the MM/GB(PB)SA method[40] are listed in Table 2 and Table S1 (ESI†). Particularly, the $\Delta G_{GB(PB)}$ values without entropy contributions for the complexes of talopram-hNET, escitalopram-hSERT, ligand**10**-hNET, ligand**10**-hSERT, talopram-hSERT, and escitalopram-hNET were −56.99(−57.78), −56.32(−56.79), −53.51(−56.49), −53.29(−57.21), −51.40(−53.45) and −50.09(−49.64) kcal mol^{-1}, respectively. The corresponding experimental binding free energies (ΔG_{exp}) of the six complexes deduced from K_i data[19] by using the equation $\Delta G_{exp} = RT\ln K_i$ were −10.64, −10.48, −9.05, −8.55, −6.21, and −5.90 kcal mol^{-1}. Obviously, the binding free energy values obtained *via* both methods were very different compared to the experimental values. It has been reported that the differences of binding free energies ($\Delta\Delta G$) were usually used to evaluate the reproducibility of ΔG_{calc} against ΔG_{exp} in many cases.[27,28,89] The correlation coefficients (R^2) between the calculated and experimental binding free energies ($\Delta\Delta G$) were 0.95 and 0.77 (Fig. 3A and B) for the MM/GBSA and MM/PBSA methods, respectively, which indicated that the former method was more suitable for the studied systems. This may be because of the more powerful properties of the MM/GBSA approach in the correct ranking of ligands with a similar scaffold.[41] The value of the entropic contributions ($-T\Delta S$) was around 21.0 kcal mol^{-1} for similar ligands binding to similar targets hNET and hSERT (Table 2 and Table S2, ESI†). After adding the entropy contributions summarized in Table 2 and Table S2 (ESI†), the overestimation of the calculated binding free energy was significantly reduced but still inevitable.[41] After the addition of the entropy contributions, the correlation coefficients (R^2) between the calculated ($\Delta G_{GB(PB).tot} = \Delta G_{GB(PB)} - T\Delta S$) and experimental binding free energies (ΔG_{exp}) were 0.93 and 0.79 (Fig. 3A′ and B′). It was obvious that the addition of entropy to the final binding free energy has a slight effect on the correlation coefficients between the calculated and experimental binding free energies. It should be noticed that only 10 frames were extracted to predict the entropy due to the very high computational demand of the calculation of entropic contributions. Therefore, in many studies, the entropy contributions were ignored due to their large computational demand and uncertainty of the calculation.[42] The entropic penalty was not taken into consideration for three main reasons. First, it has been reported that for a series of similar structures with similar binding conformations,[90,91] the entropy contribution ($-T\Delta S$) for each system may be approximately equal and the differences between each system could be ignored.[90,91] Second, the accurate calculation of ($-T\Delta S$) was computationally expensive and in many cases, its inclusion did not guarantee better accuracies in the final energies.[41] Third, the relative binding free energies could be predicted with a reasonable accuracy *via* the

Table 2 The calculated and experimental binding free energies of six studied complexes (ΔG is in kcal mol^{-1} and K_i is in nM)

Systems	ΔG_{GB}[a]	$\Delta\Delta G_{GB}$[b]	ΔG_{PB}[a]	$\Delta\Delta G_{PB}$[b]	$-T\Delta S$[c]	$\Delta G_{GB.tot}$[d]	$\Delta G_{PB.tot}$[d]	ΔG_{exp}[e]	$\Delta\Delta G_{exp}$[b]	K_i[f]
Talopram-hNET	−56.99	−6.90	−57.78	−8.14	21.18	−35.81	−36.60	−10.64	−4.74	16
Escitalopram-hSERT	−56.32	−6.23	−56.79	−7.15	21.54	−34.78	−35.25	−10.48	−4.58	21
Ligand**10**-hNET	−53.51	−3.42	−56.49	−6.85	21.01	-32.50	−35.48	−9.05	−3.15	233
Ligand**10**-hSERT	−53.29	−3.20	−57.21	−7.57	21.28	−32.01	−35.93	−8.55	−2.65	542
Talopram-hSERT	−51.40	−1.31	−53.45	−3.81	21.31	−30.09	−32.14	−6.21	−0.31	28 108
Escitalopram-hNET	−50.09	0.00	−49.64	0.00	20.23	−29.86	−29.41	−5.90	0.00	47 140

[a] Calculated MM/GB(PB)SA binding free energies based on 1000 frames in this work. [b] $\Delta\Delta G$ is defined as the change in binding free energy (ΔG) using the system of escitalopram-hNET as a reference. [c] The estimated entropic penalty based on 10 snapshots from the last 100 ns trajectory. [d] The final binding free energy calculated *via* the formula, $\Delta G_{GB(PB).tot} = \Delta G_{GB(PB)} - T\Delta S$. [e] The estimated binding free energy based on experimental K_i values by $\Delta G_{exp} = RT\ln(K_i)$. [f] Experimental K_i values from the previous study.[19]

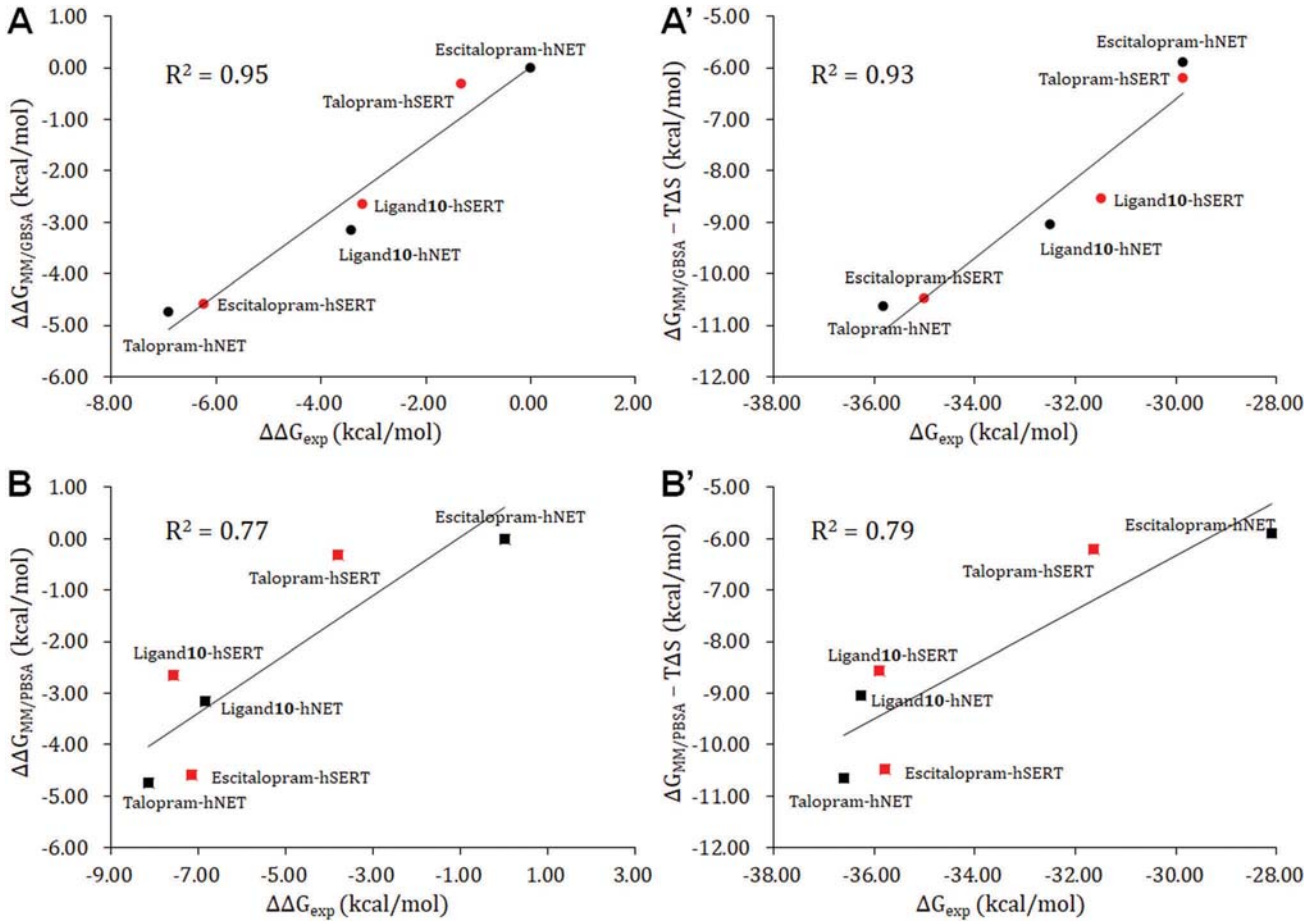

Fig. 3 The correlation coefficient (R^2) between the difference of the calculated and experimental values ($\Delta\Delta G$) using (A and A′) MM/GBSA and (B and B′) MM/PBSA methods using the escitalopram-hNET system as a reference. Compared to (A and B), the entropy change ($-T\Delta S$) was taken into consideration in (A′ and B′). Calculated binding free energy ($\Delta G_{MM/GB(PB)SA}$ or $\Delta G_{MM/GB(PB)SA} - T\Delta S$) and experimental binding free energy (ΔG_{exp}).

MM/GBSA method and it was generally sufficient to rank a series of small molecules, which was demonstrated by a large portion of the published studies.[92–94] Therefore, taking the accuracy and effectiveness into account, the binding free energies calculated without the entropy contribution[40] were an effective routine to predict the pharmaceutical activity of a series of ligands. With respect to the sampling windows of the binding free energy calculation, four different simulation windows (100–200, 200–300, 300–400, and 400–500 ns) have been sampled to compute the binding free energies and the results are summarized in Table S3 (ESI†). For clarity, the binding free energies were calculated based on the different simulation windows against the whole simulations (500 ns) and were presented in Fig. S6 (ESI†). It was clear that the MM/GBSA method reached the convergence after 500 ns simulation. Therefore, the binding free energies predicted based on 1000 snapshots from the last 100 ns trajectory (400–500 ns) had relatively high reliability and accuracy.

Secondly, the relative binding free energies of ligand**10** mutated into escitalopram and talopram in hNET and hSERT *via* TI calculation are summarized in Table 3 and Table S4 (ESI†). The results indicated the great ability of the TI method in reproducing the relative experimental free energies ($\Delta\Delta G_{exp}$). As shown, the calculated relative binding free energies ($\Delta\Delta G_{TI}$) of ligand**10** mutated into escitalopram and talopram were −3.28 and 1.03 kcal mol^{-1} in hNET, and the corresponding $\Delta\Delta G_{exp}$ were −3.15 and 1.59 kcal mol^{-1}. In hSERT, the $\Delta\Delta G_{TI}$ were 2.04 and −1.57 for ligand**10** mutated into escitalopram and talopram, while the $\Delta\Delta G_{exp}$ were 1.93 and −2.34 kcal mol^{-1}. The correlation coefficient (R^2) between the relative binding free energy ($\Delta\Delta G$) of the calculated and experimental values was 0.95 (Fig. S7, ESI†). Thirdly, the MM/3D-RISM method was employed to calculate the binding free energy of the six systems and the results were presented in Table S5 (ESI†). The details about its calculation process could be found in ESI.† Due to the huge computational demand, only 100 frames from the last 100 ns trajectory were collected. The MM/3D-RISM method has been proven to be appropriate in numerous cases, especially for the solvation of complex systems, such as complex liquid and electrolyte solutions[95] and organic supramolecular[96] and biomolecular[97] systems in solutions.[98] However, as shown in Table S5 (ESI†), the correlation coefficient (R^2) between the calculated ($\Delta\Delta G_{MM/3D\text{-}RISM}$) and experimental ($\Delta\Delta G_{exp}$) binding free energies was calculated and shown in Fig. S8 (ESI†). It indicated that the calculated binding free energies *via* MM/3D-RISM method

Table 3 The calculated and experimental binding free energies of the two mutations of ligand**10** into escitalopram and talopram in hNET and hSERT (ΔG is in kcal mol^{-1})

Systems	Mutations	FC_{K_i} [a]	$\Delta\Delta G_{exp}$ [b]	$\Delta\Delta G_{TI}$ [c]
hNET	Ligand**10** → Escitalopram	202	−3.15	−3.28
	Ligand**10** → Talopram	0.07	1.59	1.03
hSERT	Ligand**10** → Escitalopram	0.04	1.93	2.04
	Ligand**10** → Talopram	52	−2.34	−1.57

[a] FC_{K_i} indicates the fold change of two ligands based on their K_i values. [b] $\Delta\Delta G_{exp}$ is the experimental binding free energy based on experimental K_i values by $\Delta\Delta G_{exp} = -RT\ln(FC_{K_i})$. [c] $\Delta\Delta G_{TI}$ is the calculated binding free energy of the two mutation of ligands *via* the thermodynamic integration (TI) method.

could not reproduce the experimental energies. This may primarily come from the sampling. With only 100 frames collected from the last 100 ns trajectory the binding free energy could not be calculated with relatively high accuracy.

As a result, the calculated free energies using three different methods (MM/GB(PB)SA, TI and MM/3D-RISM) in this study suggested that TI calculation has a high ability in reproducing the experimental free energies of drugs escitalopram, ligand**10** and talopram binding to hNET or hSERT, while MM/GB(PB)SA and MM/3D-RISM overestimated the free energies. Interestingly, both MM/GBSA and TI demonstrated a high correlation coefficient (R^2 = 0.95 and 0.96, respectively) between the calculated and experimental relative binding free energies ($\Delta\Delta G$). Considering the effectiveness and accuracy of the calculated binding free energy, MM/GBSA per-residue energy decomposition analysis was selected for further exploring the energetic basis of drugs that selectively bind to hNET and hSERT.

Molecular determinates underlying the selective inhibition of hNET and hSERT

Escitalopram, ligand**10** and talopram shared a phenyl substituted phthalane skeleton together with a propyl amine fragment but exhibited selective inhibition of hNET and hSERT (Fig. 1). Although their binding affinities for these two targets could be distinguished by the calculated relative binding free energies, the molecular determinates for selective inhibition of hNET and hSERT resulting from the subtle modifications of the escitalopram scaffold need to be further characterized.

The conserved hot spots acting as key recognition motifs in binding sites. The total binding free energy of each complex was decomposed at the per-residue level and the residues with absolute energy contribution >0.50 kcal mol^{-1} are shown in Fig. 4. As illustrated, there were 20 and 18 key residues for inhibitors binding to hNET and hSERT, respectively. All these important residues were located within TM1, 3, 6, 8 and 10 of hNET and hSERT. Among these important residues, 2 residues on TM1 (F72 and D75 in hNET, Y95 and D98 in hSERT) and 2 residues on TM3 (V148 and Y152 in hNET, I172 and Y175 in hSERT) were identified as hot spots (with the absolute energy contribution values >2.0 kcal mol^{-1}).[99] In particular, the conserved aspartic acid in hNET (D75) and hSERT (D98), which acted as the anchor recognition sites for the ligands and determined whether ligands or chemicals belonged to the targets,[100]

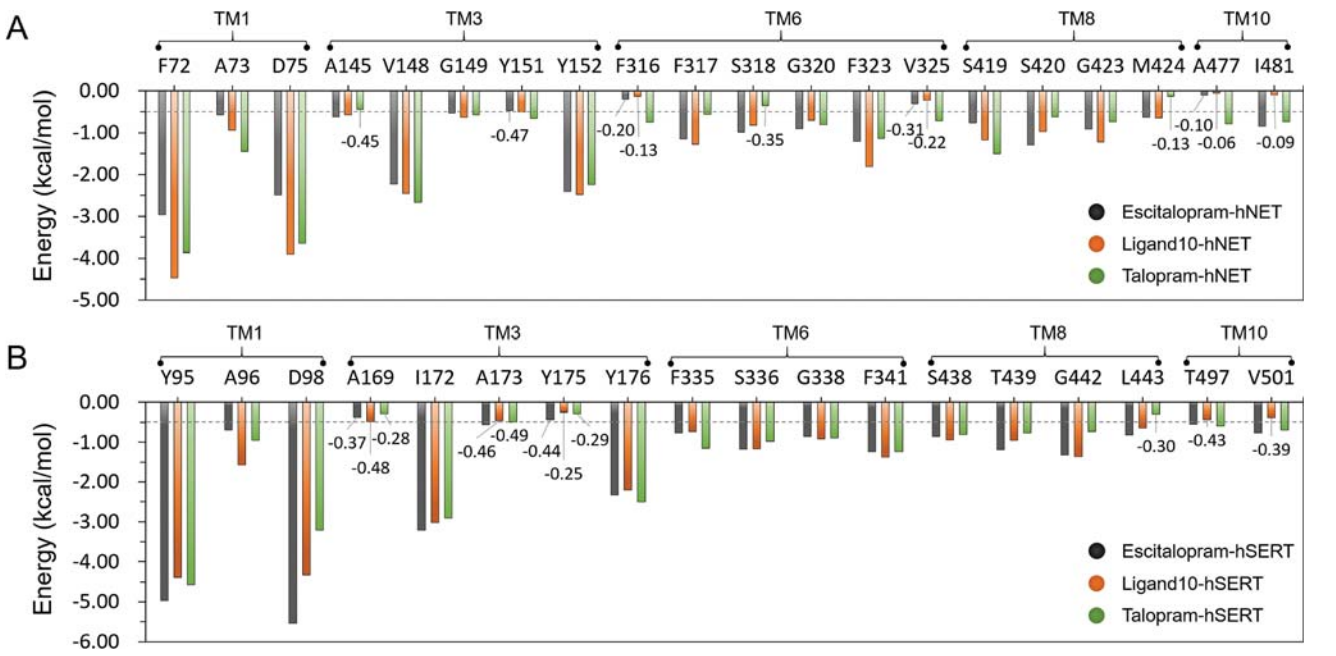

Fig. 4 Per-residue binding energy decomposition of six systems. (A) The residues with the absolute binding free energy value more than 0.50 kcal mol^{-1} are displayed in 3 hNET systems (escitalopram-hNET in black, ligand**10**-hNET in orange and talopram-hNET in green), and the transmembrane domains for these residues are labeled TM1, 3, 6, 8 and 10. (B) The residues with the absolute binding free energy value more than 0.50 kcal mol^{-1} are displayed for 3 hSERT systems (escitalopram-hSERT in black, ligand**10**-hSERT in orange and talopram-hSERT in green), and the transmembrane domains for these residues are labeled TM1, 3, 6, 8 and 10.

was identified as key residues for ligand binding in a previous study using the same method.[59] Meanwhile, energy contributions of the aspartic acid varied largely in different complexes. For the hNET bound complex, energy contributions of D75 in hNET to ligand**10** and escitalopram binding were equal to −3.90 and −2.49 kcal mol^{-1}, respectively (Fig. 4B). As shown, D98 in hSERT contributed −3.21 and −5.54 kcal mol^{-1} to the binding of talopram and escitalopram, respectively. Particularly, D75 in hNET contributed more binding energy for ligand**10** and talopram than for escitalopram, while D98 in hSERT contributed mostly to the binding of escitalopram. This difference may be related to the strength of salt bridges between the carboxyl of D75 and D98 and the charged amine group of the corresponding inhibitors. Besides, several warm spots (with absolute binding energy contributions between 0.5 and 2.0 kcal mol^{-1})[100] were identified in the binding site and interacted with different substituted inhibitors. Compared to the hot spots, warm spots might not be necessarily conserved but may regulate the ligand affinity to targets and thus affect their selectivity.[100] Therefore, molecular interaction fingerprint analysis was utilized to explore the role of warm spots in hNET and hSERT in determining the inhibitors' selective inhibition.

The roles of warm spots in hNET and hSERT in determining inhibitor selectivity. Molecular interaction fingerprints of the six studied complexes calculated by the last equilibrated 100 ns trajectories are shown in Fig. 5 and 6, respectively. For the hNET bound complex, protein–ligand interaction fingerprints demonstrated that 13 residues (F72, A73, D75, A145, V148, Y151, Y152, F323, S419, S420, M424, A477 and I481) mainly participated in 3 interaction types including ionic (salt bridge), h-bond and hydrophobic interactions with inhibitors (Table S6, ESI†). Among these residues, the conserved residue D75 interacted with the positively charged amine groups of all three inhibitors *via* ionic and h-bond interactions[59,101] and other residues formed hydrophobic contacts with other parts of inhibitors. The comparison of the protein–ligand interaction fingerprints in Fig. 5 revealed that 7 warm spots (A73, A145, Y151, S420, M424, A477 and I481) in hNET were significantly different for escitalopram, ligand**10** and talopram binding. Particularly, the interactions between 4 warm spots (A73, Y151, A477 and I481) and talopram (NRI) were preserved better than those of escitalopram (SSRI) and ligand**10** (SNRI), while the interactions between the other 2 residues (S420 and M424) and escitalopram or ligand**10** were well maintained. Thus, it could be deduced that 4 residues

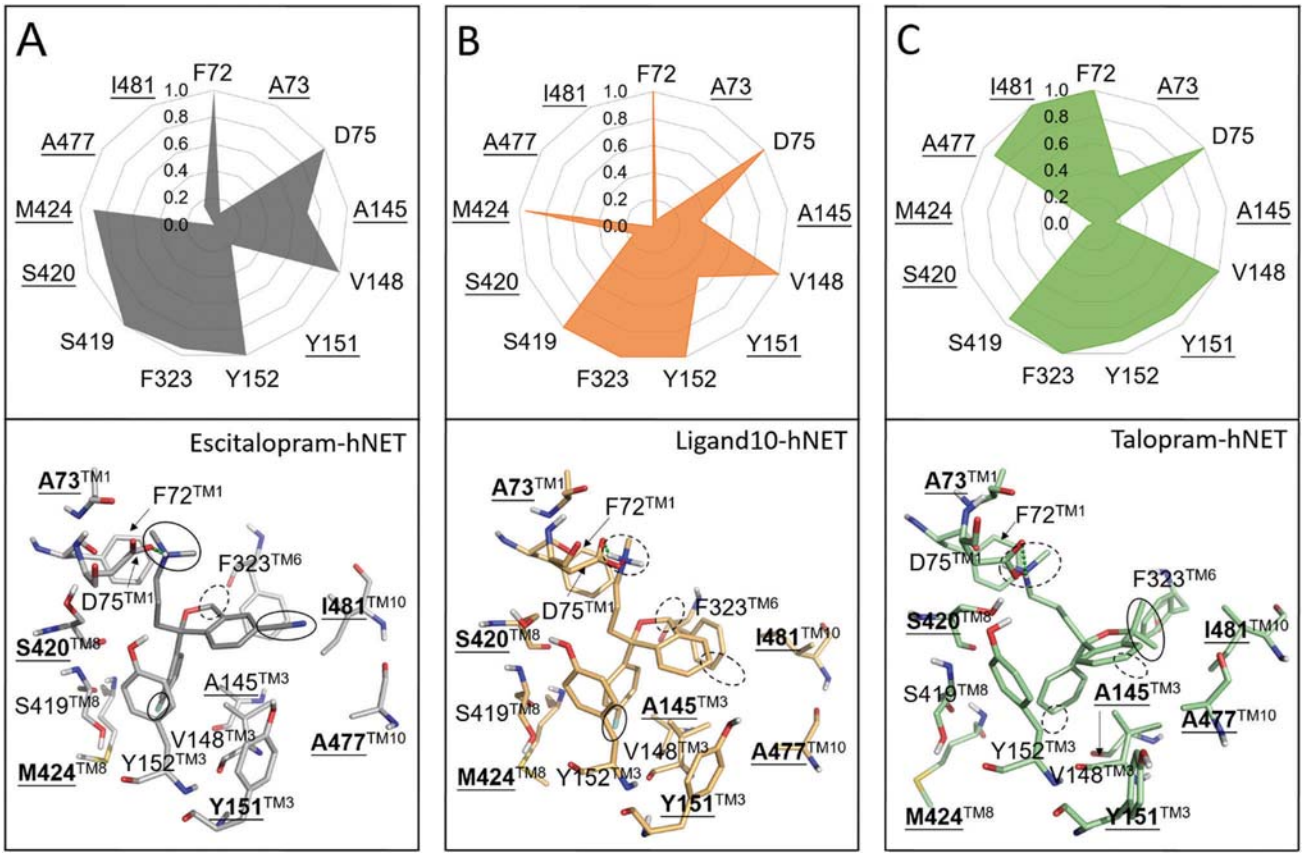

Fig. 5 The molecular interaction fingerprints between hNET and (A) escitalopram, (B) ligand**10** and (C) talopram from the last 100 ns simulations. The numbers 0–1.0 in the radar chart indicate the probability of interactions between the ligands and a certain residue based on 1000 snapshots extracted from the last 100 ns simulations. The backbones and side chains of residues and their transmembrane domains are displayed and labeled. The residues with different interaction fingerprints are underlined in bold. The four subtle modifications of the escitalopram scaffold are circled in solid and dashed lines. The solid and dashed circles indicate the presence and absence of the corresponding substituents.

(A73, Y151, A477 and I481), known as warm spots, played a crucial role in ligand selectivity for hNET. For the hSERT bound complex, 15 residues mainly engaged in 3 interaction types including ionic (salt bridge), h-bond and hydrophobic interactions with inhibitors (Table S7, ESI†). Among them, 9 warm spots (A96, A169, A173, Y175, F335, T439, L443, T497 and V501) appeared distinct in their interaction with escitalopram, ligand**10** and talopram (Fig. 6). In detail, interactions between 4 warm spots (A96, A173, T439 and L443) with escitalopram and ligand**10** were preserved better than those of talopram. These revealed that those residues had a pronounced effect on inhibitor selectivity for hSERT. However, 4 residues (A169, Y175, F335 and V501) had a minor or no effect on inhibitor binding selectivity for hSERT.

Previous studies manifested that hot spots may not be the pivotal points determining the ligand selective inhibition of protein, instead warm spots may have a significant effect on that.[100] Herein, by combining per-residue binding free energy calculation and molecular interaction fingerprint analysis, the warm spots determining the ligand selectivity for hNET and hSERT were identified and mapped on the transport proteins. As shown in Fig. 7, warm residues identified were mainly distributed on TM3, 8, and 10 domains, which were consistent with the spatial location of escitalopram scaffold modifications in the binding sites. Therefore, it is interesting to perform further thermodynamics–structure relationship analysis to understand the inhibitors' specificity for hNET and hSERT by escitalopram scaffold modifications.

Thermodynamics–structure relationship of the modified escitalopram scaffold binding to hNET and hSERT. It was known that the subtle changes on 4 positions (P1–P4) of the escitalopram scaffold could delicately affect the selectivity for hNET and hSERT[19] (Fig. 1). To reveal the relationship between the modified escitalopram scaffold and the binding free energy, a thermodynamics–structure relationship analysis was performed by displaying modifications as well as the corresponding residues' energy contribution around the substituent groups in Fig. 8 and 9 for hNET and hSERT bound complexes, respectively. Details of the residues in hNET and hSERT energy contribution are provided in Tables S8 and S9 (ESI†).

For hNET bound complexes, the dimethyl group on the escitalopram scaffold (P1) of talopram interacted with hydrophobic

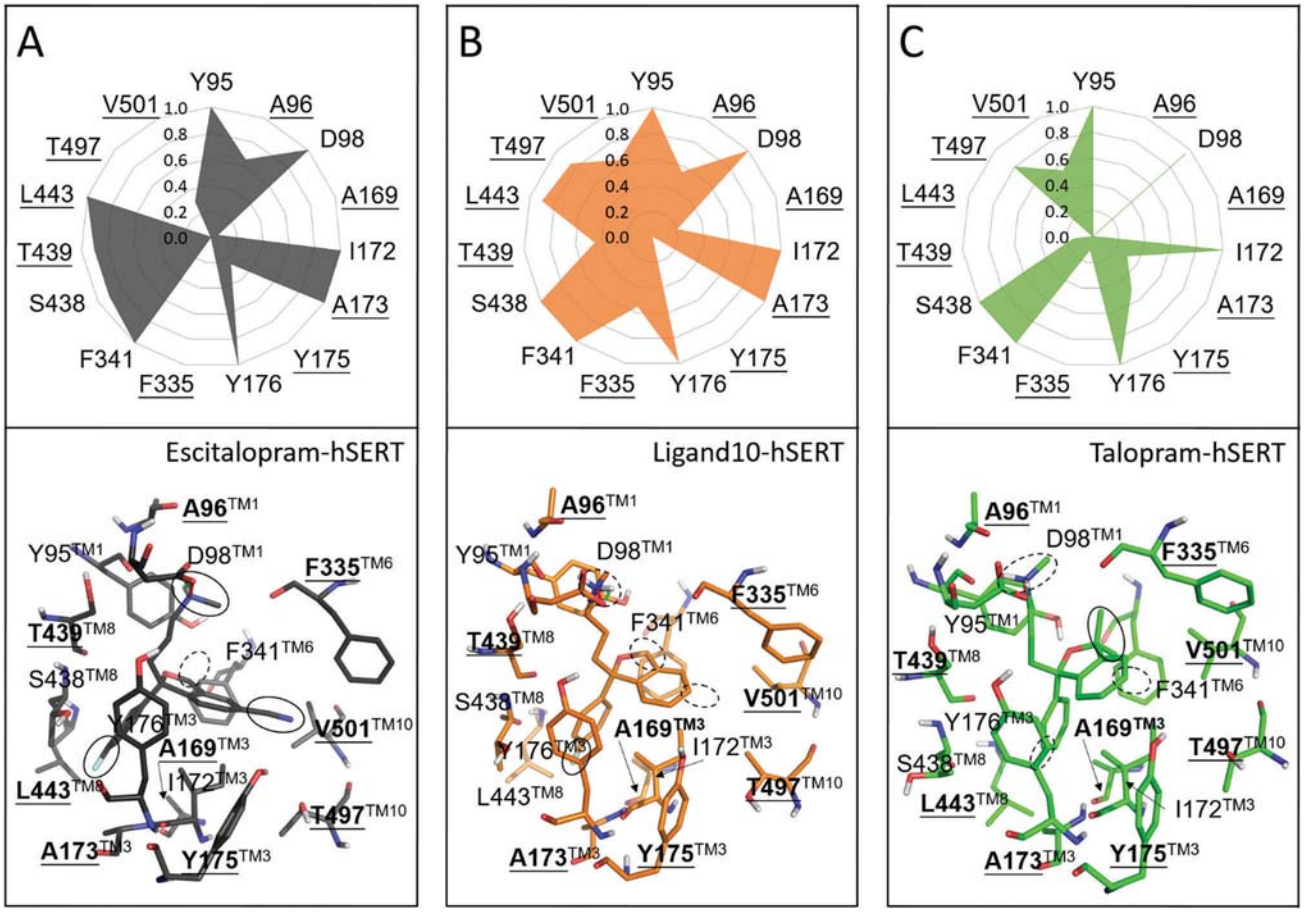

Fig. 6 The molecular interaction fingerprints between hSERT and (A) escitalopram, (B) ligand**10** and (C) talopram from the last 100 ns simulations. The numbers 0–1.0 in the radar chart indicate the probability of interactions between the ligands and a certain residue based on 1000 snapshots extracted from the last 100 ns simulations. The backbones and side chains of residues and their transmembrane domains are displayed and labeled. The residues with different interaction fingerprints are underlined in bold. The four subtle modifications of the escitalopram scaffold are circled in solid and dashed lines. The solid and dashed circles indicate the presence and absence of the corresponding substituents.

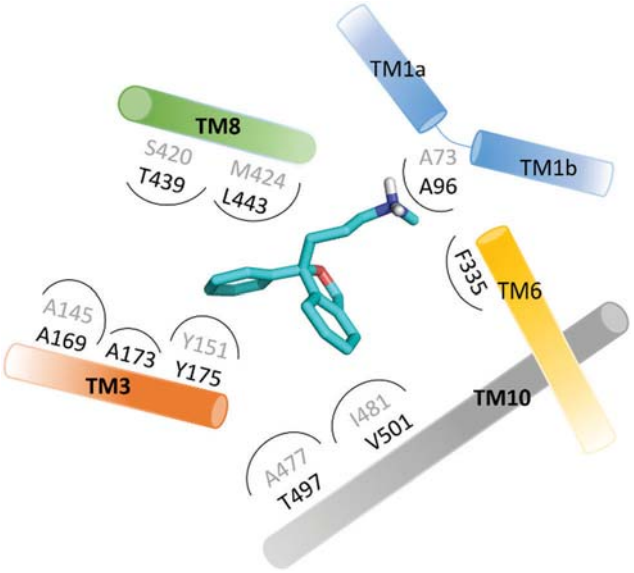

Fig. 7 Schematic description of the identified warm spots determining selective inhibition of hNET and hSERT by escitalopram scaffold modifications. Residues in hNET and hSERT are represented in grey and black colors, respectively. The escitalopram scaffold is in cyan stick. The residues distributed on TM3, 8 and 10 represented in bold mark indicate the primary effects on selective inhibition of the ligands.

residues including F316, F317, G320, F323, A477, and I481 (Fig. 8A). *Via* hydrophobic interactions, 6 residues contributed to talopram binding with an energy of -4.79 kcal mol^{-1}. The values for escitalopram and ligand**10** were -4.40 and -4.07 kcal mol^{-1}, indicating that the dimethyl group in P1 played a more important role in talopram binding to hNET. The P2 of the scaffold was inserted into a polar/apolar mixed subsite composed of one polar residue (Y151) and four apolar (V148, F317, A477 and I481) residues (Fig. 8B). Due to the more hydrophobic properties of the subsite as well as its adjacent dimethyl group in P1, residues around P2 contributed to talopram binding with the highest energy value of -5.42 kcal mol^{-1}. Additionally, compared to escitalopram and ligand**10** complexes, the benzene ring of Y151 in the talopram bound complex rotated about 90°, facilitating the hydrophobic interaction. Compared with the energy contribution to talopram binding (-5.19 kcal mol^{-1}), higher values for both escitalopram and ligand**10** (-6.22 and -6.52 kcal mol^{-1}) suggested that the introduction of fluorine (–F) to benzene in P3 was capable of enhancing the binding affinity of inhibitors to hNET (Fig. 8C). In terms of P4, the amine group interacted with the subsite formed by residues F72, A73, D75, S318, G420 and S419 (Fig. 8D). The formed tertiary group engaged in a salt bridge with the carboxyl of D75. Among the 6 residues, F72 and D75 were identified as hot spots in the previous section. Together with other 4 residues, they made contributions to escitalopram, ligand**10** and talopram with energy values of -8.68, -12.01 and -11.62 kcal mol^{-1}, respectively.

For hSERT bound complexes, the energies of residues (F335, G338 and F341) around P1 contributing to escitalopram, ligand**10** and talopram binding were -2.86, -3.03 and -3.28 kcal mol^{-1} (Fig. 9A), revealing that the attachment of a dimethyl group to P1 could slightly enhance the inhibitors' interaction with hSERT. However, more residues of hNET (F316, F317, G320, F323, A477 and I481) around P1 (Fig. 8A), and the introduction of a dimethyl group to P1 could be more beneficial to improve the inhibitor binding affinity for hNET. For P2 (Fig. 9B), escitalopram obtained

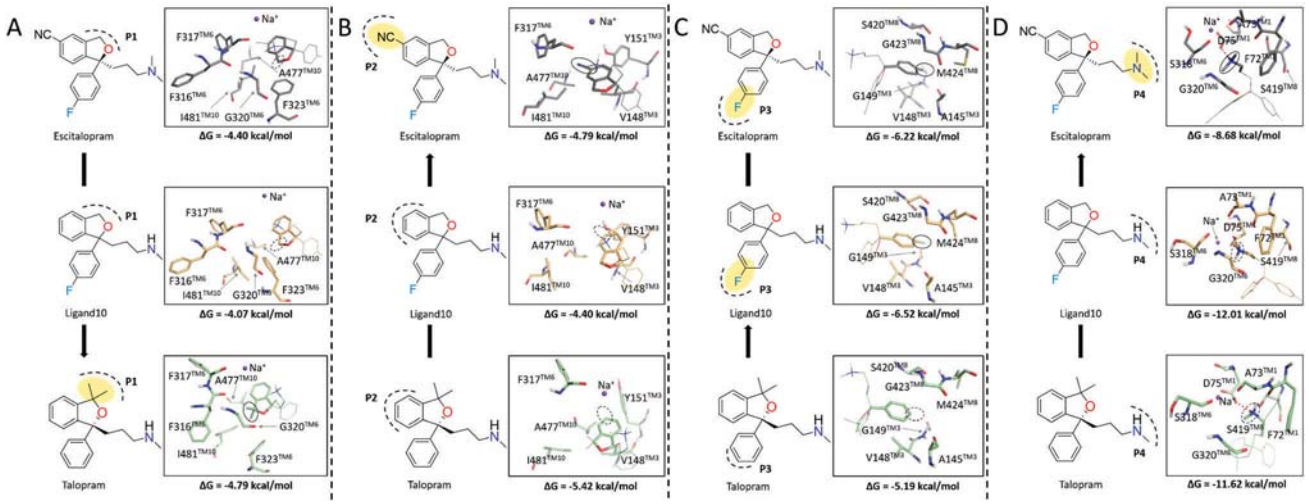

Fig. 8 Thermodynamics–structure relationships of escitalopram scaffold modifications binding to hNET. (A) P1 position modification of the escitalopram scaffold as well as the total binding free energies (ΔG) contributed by the six residues (F316, F317, G320, F323, A477 and I481) surrounding P1. (B) P2 position modification of the escitalopram scaffold as well as the total binding free energies (ΔG) contributed by the five residues (V148, Y151, F317, A477 and I481) surrounding P2. (C) P3 position modification of the escitalopram scaffold as well as the total binding free energies (ΔG) contributed by the five residues (A145, V148, G149, S420 and G423) surrounding P3. (D) P4 position modification of the escitalopram scaffold as well as the total binding free energies (ΔG) contributed by the six residues (F72, A73, D75, S318, G320 and S429) surrounding P4. The four structural modification positions P1, P2, P3 and P4 are marked as a yellow background. The representative structures of escitalopram-hNET (in grey stick), ligand**10**-hNET (in pale orange stick) and talopram-hNET (in light green stick) are extracted from the last 100 ns trajectories. The backbones and side chains of residues and their transmembrane domains are depicted and labeled.

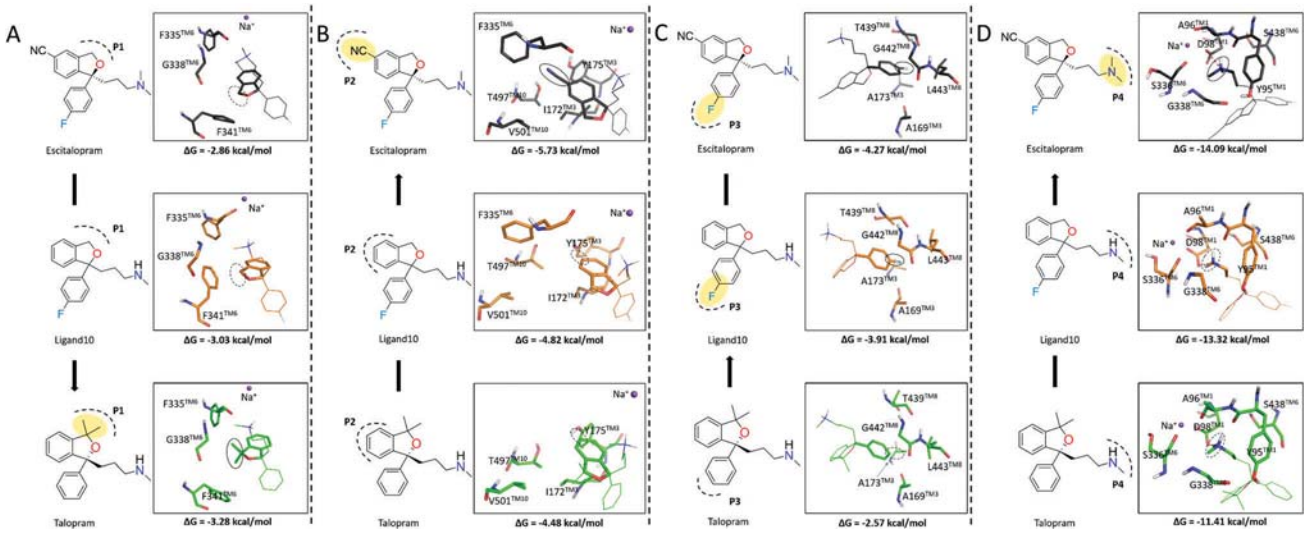

Fig. 9 Thermodynamics–structure relationships of the escitalopram scaffold modifications binding to hSERT. (A) P1 position modification of the escitalopram scaffold as well as the total binding free energies (ΔG) contributed by the three residues (F335, S338 and F341) surrounding P1. (B) P2 position modification of the escitalopram scaffold as well as the total binding free energies (ΔG) contributed by the five residues (I172, Y175, F335, T497 and V501) surrounding P2. (C) P3 position modification of the escitalopram scaffold as well as the total binding free energies (ΔG) contributed by the five residues (A169, A173, G442, T439 and L443) surrounding P3. (D) P4 position modification of the escitalopram scaffold as well as the total binding free energies (ΔG) contributed by the five residues (Y95, A96, D98, S336 and S438) surrounding P4. The four structural modification positions P1, P2, P3 and P4 are marked as a yellow background. The representative structures of escitalopram-hSERT (in black stick), ligand**10**-hSERT (in orange stick) and talopram-hSERT (in green stick) are extracted from the last 100 ns trajectories. The backbones and side chains of residues and their transmembrane domains are depicted and labeled.

the highest energy (-5.73 kcal mol^{-1}) from residues (I172, Y175, F335, T497 and V501). It was clear that, besides the hydrophobic interaction between the phenyl group and I172, Y175 and V501, the substituted cyan group (–CN) of escitalopram fitted well with polar residues Y175 and T497 (Fig. 9B). For P3, the introduction of fluorine (–F) to the benzene ring made the inhibitor establish a stronger interaction with the residues around P3 (Fig. 9C) and it was confirmed by relatively larger energy values of residues (A169, A173, G442, T439 and L443) contributing to escitalopram (-4.27 kcal mol^{-1}), ligand**10** (-3.91 kcal mol^{-1}) and talopram (-2.57 kcal mol^{-1}) binding in hSERT. In Fig. 9D, the tertiary amine in escitalopram participated in a salt bridge with the carboxyl of D98 and the residues (A96, Y95, D98, S336, G338, S438) collectively contributed to this moiety with the highest energy (-14.09 kcal mol^{-1}), while the contribution to the second amine of ligand**10** and talopram was -13.32 and -11.41 kcal mol^{-1}.

The above thermodynamics–structure relationship demonstrated that the subtle changes on the P1–P4 of the escitalopram scaffold obtained different binding free energy contributions from subsite residues of the target, which to a certain level quantitatively reflected the selective inhibition of hNET and hSERT by escitalopram scaffold modifications. Moreover, based on the thermodynamics–structure relationship analysis, some general insight can be summarized for selective inhibition of hNET and hSERT. For hNET, (i) the dimethyl group substituted at P1 of the escitalopram scaffold tended to exhibit more hNET inhibitory activity; (ii) the cyan group at P2 of the scaffold was not favorable for hNET inhibitory activity, while it was inclined to display hSERT inhibitory activity; (iii) fluorine attached to P3 of the benzene ring may enhance the ligand affinity for hNET; (iv) the second amine group at P4 was preferable to tertiary amine in hNET. For hSERT, (i) the dimethyl group attached to P1 of the scaffold could improve the ligand affinity for hSERT but result in higher affinity for hNET; (ii) the cyan group at P2 was more facilitated to enhance the ligand affinity for hSERT; (iii) the fluorine attached to the P3 of the benzene ring could also enhance the ligand affinity for hSERT; (iv) the tertiary amine group was inclined to exhibit higher affinity for hSERT.

Conclusions

In this study, three ligands (escitalopram, ligand**10** and talopram) were adopted as probes to investigate the selective inhibition of hNET and hSERT. Computational methods such as homology modeling, molecular docking and MD simulations, followed by free energy calculations, molecular interaction fingerprints and thermodynamics–structure relationship analysis were integrated to investigate selective inhibition of hNET and hSERT. The calculated free energies using three different methods (MM/GB(PB)SA, TI and MM/3D-RISM) suggested that TI calculation has a high capacity of reproducing the experimental free energies of escitalopram, ligand**10** and talopram binding to hNET or hSERT, while MM/GB(PB)SA and MM/3D-RISM overestimated the binding free energy. Among them, the MM/GBSA method has the advantages of relative accuracy and efficiency. As a result, 4 warm spots (A73, Y151, A477 and I481) in hNET and 4 warm spots (A96, A173, T439 and L443) in hSERT had a pronounced effect on the ligand selectivity. These simulation results would shed light on the residues affecting inhibitor selectivity in these two highly similar transporters, providing great insight into the

design of inhibitors with the desired selectivity to hNET and hSERT and further promoting the research of more efficacious antidepressants.

Conflicts of interest

There are no conflicts to declare.

Acknowledgements

This work was funded by the National Natural Science Foundation of China (81872798 and 21505009), the Innovation Project on Industrial Generic Key Technologies of Chongqing (cstc2015zdcy-ztzx120003), and the Fundamental Research Funds for Central Universities (10611CDJXZ238826, CDJZR14468801, CDJKXB14011, 2015CDJXY and 2018CDQYSG0007).

References

1 R. Santos, O. Ursu, A. Gaulton, A. P. Bento, R. S. Donadi, C. G. Bologa, A. Karlsson, B. Al-Lazikani, A. Hersey, T. I. Oprea and J. P. Overington, *Nat. Rev. Drug Discovery*, 2017, **16**, 19–34.
2 Y. H. Li, C. Y. Yu, X. X. Li, P. Zhang, J. Tang, Q. Yang, T. Fu, X. Zhang, X. Cui, G. Tu, Y. Zhang, S. Li, F. Yang, Q. Sun, C. Qin, X. Zeng, Z. Chen, Y. Z. Chen and F. Zhu, *Nucleic Acids Res.*, 2018, **46**, D1121–D1127.
3 F. Zhu, X. X. Li, S. Y. Yang and Y. Z. Chen, *Trends Pharmacol. Sci.*, 2018, **39**, 229–231.
4 A. S. Kristensen, J. Andersen, T. N. Jorgensen, L. Sorensen, J. Eriksen, C. J. Loland, K. Stromgaard and U. Gether, *Pharmacol. Rev.*, 2011, **63**, 585–640.
5 A. B. Pramod, J. Foster, L. Carvelli and L. K. Henry, *Mol. Aspects Med.*, 2013, **34**, 197–219.
6 S. Manepalli, C. K. Surratt, J. D. Madura and T. L. Nolan, *AAPS J.*, 2012, **14**, 820–831.
7 J. Fu, J. Tang, Y. Wang, X. Cui, Q. Yang, J. Hong, X. Li, S. Li, Y. Chen, W. Xue and F. Zhu, *Front. Pharmacol.*, 2018, **9**, 681.
8 J. Andersen, N. Stuhr-Hansen, L. G. Zachariassen, H. Koldso, B. Schiott, K. Stromgaard and A. S. Kristensen, *Mol. Pharmacol.*, 2014, **85**, 703–714.
9 P. Wang, F. Yang, H. Yang, X. Xu, D. Liu, W. Xue and F. Zhu, *Bio-Med. Mater. Eng.*, 2015, **26**(suppl 1), S2233–S2239.
10 F. Zhu, B. Han, P. Kumar, X. Liu, X. Ma, X. Wei, L. Huang, Y. Guo, L. Han, C. Zheng and Y. Chen, *Nucleic Acids Res.*, 2010, **38**, D787–D791.
11 P. K. Gillman, *Br. J. Pharmacol.*, 2007, **151**, 737–748.
12 F. Zhu, Z. Shi, C. Qin, L. Tao, X. Liu, F. Xu, L. Zhang, Y. Song, X. Liu, J. Zhang, B. Han, P. Zhang and Y. Chen, *Nucleic Acids Res.*, 2012, **40**, D1128–D1136.
13 F. Zhu, L. Han, C. Zheng, B. Xie, M. T. Tammi, S. Yang, Y. Wei and Y. Chen, *J. Pharmacol. Exp. Ther.*, 2009, **330**, 304–315.
14 M. J. Owens, D. L. Knight and C. B. Nemeroff, *Biol. Psychiatry*, 2001, **50**, 345–350.
15 J. N. Eildal, J. Andersen, A. S. Kristensen, A. M. Jorgensen, B. Bang-Andersen, M. Jorgensen and K. Stromgaard, *J. Med. Chem.*, 2008, **51**, 3045–30458.
16 E. Dale, B. Bang-Andersen and C. Sanchez, *Biochem. Pharmacol.*, 2015, **95**, 81–97.
17 L. Iversen, *Mol. Psychiatry*, 2000, **5**, 357–362.
18 P. F. Saltiel and D. I. Silvershein, *Neuropsychiatr. Dis. Treat.*, 2015, **11**, 875–888.
19 J. Andersen, N. Stuhr-Hansen, L. Zachariassen, S. Toubro, S. M. Hansen, J. N. Eildal, A. D. Bond, K. P. Bogeso, B. Bang-Andersen, A. S. Kristensen and K. Stromgaard, *Proc. Natl. Acad. Sci. U. S. A.*, 2011, **108**, 12137–12142.
20 Z. J. Han, W. W. Xue, L. Tao and F. Zhu, *CNS Neurosci. Ther.*, 2018, **24**, 1253–1263.
21 R. Mandrioli, L. Mercolini, M. A. Saracino and M. A. Raggi, *Curr. Med. Chem.*, 2012, **19**, 1846–1863.
22 J. A. Coleman, E. M. Green and E. Gouaux, *Nature*, 2016, **532**, 334–339.
23 J. Grouleff, L. K. Ladefoged, H. Koldso and B. Schiott, *Front. Pharmacol.*, 2015, **6**, 235.
24 H. Koldsø, K. Severinsen, T. T. Tran, L. Celik, H. H. Jensen, O. Wiborg, B. Schiott and S. Sinning, *J. Am. Chem. Soc.*, 2010, **132**, 1311–1322.
25 A. Yamashita, S. K. Singh, T. Kawate, Y. Jin and E. Gouaux, *Nature*, 2005, **437**, 215–223.
26 A. Penmatsa, K. H. Wang and E. Gouaux, *Nature*, 2013, **503**, 85–90.
27 W. Xue, P. Wang, B. Li, Y. Li, X. Xu, F. Yang, X. Yao, Y. Z. Chen, F. Xu and F. Zhu, *Phys. Chem. Chem. Phys.*, 2016, **18**, 3260–3271.
28 G. Zheng, W. Xue, P. Wang, F. Yang, B. Li, X. Li, Y. Li, X. Yao and F. Zhu, *Sci. Rep.*, 2016, **6**, 26883.
29 W. Xue, F. Yang, P. Wang, G. Zheng, Y. Chen, X. Yao and F. Zhu, *ACS Chem. Neurosci.*, 2018, **9**, 1128–1140.
30 W. Xue, P. Wang, G. Tu, F. Yang, G. Zheng, X. Li, X. Li, Y. Chen, X. Yao and F. Zhu, *Phys. Chem. Chem. Phys.*, 2018, **20**, 6606–6616.
31 W. L. Jorgensen, *Acc. Chem. Res.*, 2009, **42**, 724–733.
32 M. R. Reddy, C. R. Reddy, R. S. Rathore, M. D. Erion, P. Aparoy, R. N. Reddy and P. Reddanna, *Curr. Pharm. Des.*, 2014, **20**, 3323–3337.
33 L. Wang, Y. Wu, Y. Deng, B. Kim, L. Pierce, G. Krilov, D. Lupyan, S. Robinson, M. K. Dahlgren, J. Greenwood, D. L. Romero, C. Masse, J. L. Knight, T. Steinbrecher, T. Beuming, W. Damm, E. Harder, W. Sherman, M. Brewer, R. Wester, M. Murcko, L. Frye, R. Farid, T. Lin, D. L. Mobley, W. L. Jorgensen, B. J. Berne, R. A. Friesner and R. Abel, *J. Am. Chem. Soc.*, 2015, **137**, 2695–2703.
34 M. Ciordia, L. Perez-Benito, F. Delgado, A. A. Trabanco and G. Tresadern, *J. Chem. Inf. Model.*, 2016, **56**, 1856–1871.
35 R. Abel, L. Wang, E. D. Harder, B. J. Berne and R. A. Friesner, *Acc. Chem. Res.*, 2017, **50**, 1625–1632.
36 T. Fu, G. Zheng, G. Tu, F. Yang, Y. Chen, X. Yao, X. Li, W. Xue and F. Zhu, *ACS Chem. Neurosci.*, 2018, **9**, 1492–1502.
37 T. S. Lee, Y. Hu, B. Sherborne, Z. Guo and D. M. York, *J. Chem. Theory Comput.*, 2017, **13**, 3077–3084.
38 T. J. Giese and D. M. York, *J. Chem. Theory Comput.*, 2018, **14**, 1564–1582.
39 S. Genheden, T. Luchko, S. Gusarov, A. Kovalenko and U. Ryde, *J. Phys. Chem. B*, 2010, **114**, 8505–8516.

40 S. Genheden and U. Ryde, *Expert Opin. Drug Discovery*, 2015, **10**, 449–461.
41 T. Hou, J. Wang, Y. Li and W. Wang, *J. Chem. Inf. Model.*, 2011, **51**, 69–82.
42 H. Sun, Y. Li, S. Tian, L. Xu and T. Hou, *Phys. Chem. Chem. Phys.*, 2014, **16**, 16719–16729.
43 G. Zeller, J. Tap, A. Y. Voigt, S. Sunagawa, J. R. Kultima, P. I. Costea, A. Amiot, J. Bohm, F. Brunetti, N. Habermann, R. Hercog, M. Koch, A. Luciani, D. R. Mende, M. A. Schneider, P. Schrotz-King, C. Tournigand, J. Tran Van Nhieu, T. Yamada, J. Zimmermann, V. Benes, M. Kloor, C. M. Ulrich, M. von Knebel Doeberitz, I. Sobhani and P. Bork, *Mol. Syst. Biol.*, 2014, **10**, 766.
44 F. Chen, H. Liu, H. Sun, P. Pan, Y. Li, D. Li and T. Hou, *Phys. Chem. Chem. Phys.*, 2016, **18**, 22129–22139.
45 H. Sun, L. Duan, F. Chen, H. Liu, Z. Wang, P. Pan, F. Zhu, J. Z. H. Zhang and T. Hou, *Phys. Chem. Chem. Phys.*, 2018, **20**, 14450–14460.
46 B. Li, J. Tang, Q. Yang, X. Cui, S. Li, S. Chen, Q. Cao, W. Xue, N. Chen and F. Zhu, *Sci. Rep.*, 2016, **6**, 38881.
47 Y. H. Li, J. Y. Xu, L. Tao, X. F. Li, S. Li, X. Zeng, S. Y. Chen, P. Zhang, C. Qin, C. Zhang, Z. Chen, F. Zhu and Y. Z. Chen, *PLoS One*, 2016, **11**, e0155290.
48 L. Tao, F. Zhu, F. Xu, Z. Chen, Y. Y. Jiang and Y. Z. Chen, *Pharmacol. Res.*, 2015, **102**, 123–131.
49 PyMOL Molecular Graphics System, 1.3, Schrödinger, LLC, New York, NY, 2009.
50 Protein Preparation Wizard, Schrödinger, LLC, New York, NY, 2009.
51 Prime, 3.1, Schrödinger, LLC, New York, NY, 2009.
52 T. Pacholczyk, R. D. Blakely and S. G. Amara, *Nature*, 1991, **350**, 350–354.
53 M. A. Larkin, G. Blackshields, N. P. Brown, R. Chenna, P. A. McGettigan, H. McWilliam, F. Valentin, I. M. Wallace, A. Wilm, R. Lopez, J. D. Thompson, T. J. Gibson and D. G. Higgins, *Bioinformatics*, 2007, **23**, 2947–2948.
54 X. Robert and P. Gouet, *Nucleic Acids Res.*, 2014, **42**, W320–W324.
55 I. W. Davis, A. Leaver-Fay, V. B. Chen, J. N. Block, G. J. Kapral, X. Wang, L. W. Murray, W. B. Arendall, J. Snoeyink, J. S. Richardson and D. C. Richardson, *Nucleic Acids Res.*, 2007, **35**, W375–W383.
56 Glide, 5.5, Schrödinger, LLC, New York, NY, 2009.
57 D. J. Price and C. L. Brooks, 3rd, *J. Comput. Chem.*, 2005, **26**, 1529–1541.
58 Epik, 2.0, Schrödinger, LLC, New York, NY, 2009.
59 L. Sorensen, J. Andersen, M. Thomsen, S. M. Hansen, X. Zhao, A. Sandelin, K. Stromgaard and A. S. Kristensen, *J. Biol. Chem.*, 2012, **287**, 43694–44707.
60 C. Y. Yu, X. X. Li, H. Yang, Y. H. Li, W. W. Xue, Y. Z. Chen, L. Tao and F. Zhu, *Int. J. Mol. Sci.*, 2018, **19**, 183.
61 J. Xu, P. Wang, H. Yang, J. Zhou, Y. Li, X. Li, W. Xue, C. Yu, Y. Tian and F. Zhu, *BioMed Res. Int.*, 2016, 2509385.
62 F. Zhu, L. Y. Han, X. Chen, H. H. Lin, S. Ong, B. Xie, H. L. Zhang and Y. Z. Chen, *Curr. Protein Pept. Sci.*, 2008, **9**, 70–95.
63 M. A. Lomize, I. D. Pogozheva, H. Joo, H. I. Mosberg and A. L. Lomize, *Nucleic Acids Res.*, 2012, **40**, D370–D376.
64 E. L. Wu, X. Cheng, S. Jo, H. Rui, K. C. Song, E. M. Davila-Contreras, Y. Qi, J. Lee, V. Monje-Galvan, R. M. Venable, J. B. Klauda and W. Im, *J. Comput. Chem.*, 2014, **35**, 1997–2004.
65 W. L. Jorgensen, J. Chandrasekhar, J. D. Madura, R. W. Impey and M. L. Klein, *J. Chem. Phys.*, 1983, **79**, 926–935.
66 AMBER 16, University of California, San Francisco, 2016.
67 C. J. Dickson, B. D. Madej, A. A. Skjevik, R. M. Betz, K. Teigen, I. R. Gould and R. C. Walker, *J. Chem. Theory Comput.*, 2014, **10**, 865–879.
68 I. S. Joung and T. E. Cheatham, *J. Phys. Chem. B*, 2009, **113**, 13279–13290.
69 F. Yang, G. Zheng, T. Fu, X. Li, G. Tu, Y. H. Li, X. Yao, W. Xue and F. Zhu, *Phys. Chem. Chem. Phys.*, 2018, **20**, 23873–23884.
70 J. Wang, W. Wang, P. A. Kollman and D. A. Case, *J. Mol. Graphics Modell.*, 2006, **25**, 247–260.
71 P. R. Maycox, F. Kelly, A. Taylor, S. Bates, J. Reid, R. Logendra, M. R. Barnes, C. Larminie, N. Jones, M. Lennon, C. Davies, J. J. Hagan, C. A. Scorer, C. Angelinetta, M. T. Akbar, S. Hirsch, A. M. Mortimer, T. R. Barnes and J. de Belleroche, *Mol. Psychiatry*, 2009, **14**, 1083–1094.
72 R. W. Pastor, B. R. Brooks and A. Szabo, *Mol. Phys.*, 1988, **65**, 1409–1419.
73 H. G. Petersen, *J. Chem. Phys.*, 1995, **103**, 3668–3679.
74 S. Miyamoto and P. A. Kollman, *J. Comput. Chem.*, 1992, **13**, 952–962.
75 A. Onufriev, D. Bashford and D. A. Case, *Proteins*, 2004, **55**, 383–394.
76 J. Wang, P. Morin, W. Wang and P. A. Kollman, *J. Am. Chem. Soc.*, 2001, **123**, 5221–5230.
77 J. Weiser, P. S. Shenkin and W. C. Still, *J. Comput. Chem.*, 1999, **20**, 217–230.
78 Y. H. Li, P. P. Wang, X. X. Li, C. Y. Yu, H. Yang, J. Zhou, W. W. Xue, J. Tan and F. Zhu, *PLoS One*, 2016, **11**, e0165737.
79 I. Bahar, T. R. Lezon, A. Bakan and I. H. Shrivastava, *Chem. Rev.*, 2010, **110**, 1463–1497.
80 J. Chen, X. Wang, T. Zhu, Q. Zhang and J. Z. Zhang, *J. Chem. Inf. Model.*, 2015, **55**, 1903–1913.
81 J. Desaphy, E. Raimbaud, P. Ducrot and D. Rognan, *J. Chem. Inf. Model.*, 2013, **53**, 623–637.
82 B. Li, J. Tang, Q. Yang, S. Li, X. Cui, Y. Li, Y. Chen, W. Xue, X. Li and F. Zhu, *Nucleic Acids Res.*, 2017, **45**, W162–W170.
83 F. Zhu, C. J. Zheng, L. Y. Han, B. Xie, J. Jia, X. Liu, M. T. Tammi, S. Y. Yang, Y. Q. Wei and Y. Z. Chen, *Curr. Mol. Pharmacol.*, 2008, **1**, 213–232.
84 G. Marcou and D. Rognan, *J. Chem. Inf. Model.*, 2007, **47**, 195–207.
85 Y. Haddad, Z. Heger and V. Adam, *ACS Chem. Neurosci.*, 2016, **7**, 1607–1613.
86 L. R. Forrest, S. Tavoulari, Y. W. Zhang, G. Rudnick and B. Honig, *Proc. Natl. Acad. Sci. U. S. A.*, 2007, **104**, 12761–12766.
87 H. B. Rao, F. Zhu, G. B. Yang, Z. R. Li and Y. Z. Chen, *Nucleic Acids Res.*, 2011, **39**, W385–W390.
88 F. Zhu, X. H. Ma, C. Qin, L. Tao, X. Liu, Z. Shi, C. L. Zhang, C. Y. Tan, Y. Z. Chen and Y. Y. Jiang, *PLoS One*, 2012, **7**, e39782.

89 F. Y. Yang, T. T. Fu, X. Y. Zhang, J. Hu, W. W. Xue, G. X. Zheng, B. Li, Y. H. Li, X. J. Yao and F. Zhu, *Mol. Simul.*, 2017, **43**, 1089–1098.
90 G. Klebe, *Nat. Rev. Drug Discovery*, 2015, **14**, 95–110.
91 A. Ganesan, M. L. Coote and K. Barakat, *Drug Discovery Today*, 2017, **22**, 249–269.
92 P. Wang, X. Zhang, T. Fu, S. Li, B. Li, W. Xue, X. Yao, Y. Chen and F. Zhu, *ACS Chem. Neurosci.*, 2017, **8**, 1416–1428.
93 P. Wang, T. Fu, X. Zhang, F. Yang, G. Zheng, W. Xue, Y. Chen, X. Yao and F. Zhu, *Biochim. Biophys. Acta*, 2017, **1861**, 2766–2777.
94 H. Yang, C. Qin, Y. H. Li, L. Tao, J. Zhou, C. Y. Yu, F. Xu, Z. Chen, F. Zhu and Y. Z. Chen, *Nucleic Acids Res.*, 2016, **44**, D1069–D1074.
95 I. S. Joung, T. Luchko and D. A. Case, *J. Chem. Phys.*, 2013, **138**, 044103.
96 J. Phanich, T. Rungrotmongkol, D. Sindhikara, S. Phongphanphanee, N. Yoshida, F. Hirata, N. Kungwan and S. Hannongbua, *Protein Sci.*, 2016, **25**, 147–158.
97 M. Sugita and F. Hirata, *J. Phys.: Condens. Matter*, 2016, **28**, 384002.
98 T. Luchko, S. Gusarov, D. R. Roe, C. Simmerling, D. A. Case, J. Tuszynski and A. Kovalenko, *J. Chem. Theory Comput.*, 2010, **6**, 607–624.
99 D. R. Hall, D. Kozakov, A. Whitty and S. Vajda, *Trends Pharmacol. Sci.*, 2015, **36**, 724–736.
100 P. C. Rathi, R. F. Ludlow, R. J. Hall, C. W. Murray, P. N. Mortenson and M. L. Verdonk, *J. Med. Chem.*, 2017, **60**, 4036–4046.
101 H. Wang, A. Goehring, K. H. Wang, A. Penmatsa, R. Ressler and E. Gouaux, *Nature*, 2013, **503**, 141–145.